ARTICLE

Structural Analysis of Pentacene Thin Film Growth on Polycrystalline O_x–Au Surfaces Using Scanning Tunneling Microscopy

Yi Zheng,[†,*] Andrew Thye Shen Wee,[†] and Natarajan Chandrasekhar[‡,*]

[†]Department of Physics, National University of Singapore, 2 Science Drive 3, Singapore 117542 and [‡]Institute of Material Research and Engineering (IMRE), 3 Research Link, Singapore 117602

ABSTRACT In this letter, we show the feasibility to use scanning tunneling microscopy (STM) as a stand-alone technique in analyzing the structure of organic thin films grown on polycrystalline metal surfaces. At room temperature, by effectively suppressing the molecule–substrate interaction, pentacene resumes the typical quasi layer-by-layer growth with the "thin-film phase" structure due to intermolecule interaction, while substrate roughness does not play an important role. By elevating the substrate to 320 K, two different polycrystalline phases, that is, the "thin-film phase" and the "single-crystal phase" intermixed grow and form terraced and lamellar structures, respectively. Using STM distance–voltage spectroscopy, the energy level alignment of the underlying organic/metal interfaces can also be acquired.

KEYWORDS: pantacene · thin film growth · structural analysis · STM

Thin film growth of organic molecules on metal substrates is a critical step for fabricating molecular electronic devices, such as organic light-emitting diodes (OLEDs) and organic thin-film transistors (OTFTs). Because of competing parameters such as intermolecule interaction, molecule–substrate interaction, substrate temperature and roughness, and deposition rate, molecules can pack in different crystallographic configurations with similar lattice energy, that is, packing polymorphism.[1] Consequently, organic thin films may have different microcrystalline phases mixed together[2,3] or change its polymorphs as thickness increases.[4,5] One straightforward way to distinguish different polymorphs would be using characterization techniques with molecular/atomic resolution, such as scanning tunneling microscopy (STM).

However, despite its great success in studying inorganic thin film growth, STM is generally thought not suitable for studying organic thin films above the first few monolayers. One major concern is the high surface roughness of organic thin films due to dominant Stranski–Krastanov or quasi layer-by-layer growth.[1] STM study of organic thin film is also impeded by the poor conductivity of organic thin films and by tip contamination when weakly bound molecules in organic thin film are picked up by the STM tip during image acquisition. Thus, only few STM studies on organic thin film growth have been reported.[6]

In this study, we analyze the thin film structure of pentacene (Pn) grown on slightly oxidized polycrystalline O_x–Au surfaces using STM as a main characterization technique. By suppressing the interfacial molecule–substrate interaction using slight surface oxidation, intermolecule interaction dominates the thin film growth and Pn grows in a quasi layer-by-layer fashion with the "thin-film phase" structure, despite the fact that the substrates have rather rough surfaces. Packing polymorphism can be observed when the substrate temperature is elevated from room temperature to 320 K. At this temperature, terraced and lamellar structures, corresponding to the "thin-film phase" and the "single-crystal phase" respectively, are intermixed and grow with slightly different lattice parameters. Besides the surface morphology, we have used STM distance-voltage spectroscopy to determine the energy level alignment at the underlying Pn/O_x–Au interface, which is ohmic with a hole injection barrier that is $<$0.3 eV. The experimental results have been repeated on three different batches of samples.

RESULTS AND DISCUSSION

We first study Pn growth on room temperature (RT) O_x–Au surfaces. To

*Address correspondence to phyzy@nus.edu.sg, n-chandra@imre.a-star.edu.sg.

Received for review October 29, 2009 and accepted March 17, 2010.

Published online March 29, 2010. 10.1021/nn9015218

keep the O_x−Au substrates at 293 K (monitored by a thermal couple), the sample holder, equipped with an independent cryogenic loop isolated from the main vacuum chamber, was cooled by continuous RT N_2 gas flowing during organic deposition. Under such conditions, Pn thin films show the typical faceted-terrace structures, as shown in Figure 1a. From the line section crossing single domains (Figure 1b), molecular steps of ~1.5 nm are determined. Combining the faceted-terrace structures[9] and the molecular step height,[8,10] we can conclude that Pn molecules stand up on the surface and form the thin-film phase structures (Figure 1c), which is further confirmed by near edge X-ray absorption spectroscopy (NEXAFS) with an average molecular tilt angle of 77 ± 5° (see Supporting Information). The formation of the thin-film phase structures is closely related to the fractal growth of Pn molecules on inert surfaces due to dominant intermolecule interactions.[8,11] In sharp contrast, when substrate−molecule interaction dominates, such as Pn on clean Au(111) surfaces[10,12] and on air exposed polycrystalline Au surfaces (air−Au),[3] molecules tend to lie down on the surface and form microcrystalline phases. The difference between O_x−Au and untreated Au surfaces comes from the slight surface oxidation introduced by oxygen plasma treatment, which effectively suppresses the metal−molecule interaction. Such a treatment is as effective as covering the Au surfaces by self-assembled monolayers (SAM), on which Pn thin films show identical surface morphology as on O_x−Au (C8-alkanethiol SAM covered Au(111) surfaces were used in this study).

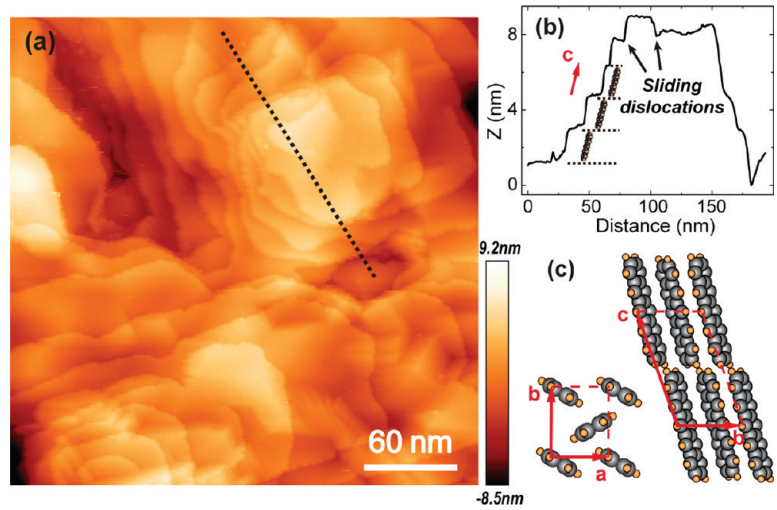

Figure 1. (a) STM image of Pn thin film on RT O_x−Au substrate, showing the dominant faceted-terrace structures. More than 10 monolayers can be resolved in this image. Scanning parameters: 300 × 300 nm²; V_{tip} = 3 V, I_t = 15pA. (b) Line section crossing one single domain showing 1.5 nm molecular steps and sliding dislocations. (c) Unit cell of the single-crystal phase and thin-film phase. The single-crystal phase has a triclinic lattice structure with a = 7.93 Å, b = 6.14 Å, c = 16.03 Å, α = 101.9°, β = 112.6°, and γ = 85.8°.[7] For the thin-film phase, a, b, and c are changed to 7.58, 5.91, and 15.4 Å respectively, while γ is nearly 90°.[7,8]

Thus, using STM, we have proven that the O_2-plasma treatment of Au surfaces can effectively decouple the molecule−substrate interaction and yield the typical quasi-layer-by-layer growth of Pn with the thin-film phase structure due to dominant intermolecule interaction. However, compared to Pn growth on flat inert surfaces such as SiO_2 and PEDOT/PSS,[8] the domain size of Pn on O_x−Au is much reduced, which is due to the surface roughness of polycrystalline Au. One possible explanation would be that rough surfaces trap Pn molecules locally and increase nucleation centers for thin film growth.[8,11] Similar surface roughness induced decrease in Pn grain sizes has also been observed on SAM-modified oxide surfaces, which is reviewed in ref 8. Another noticeable effect of surface roughness on Pn thin film growth is that it makes Pn molecules slide along the c axis ([001]) while retaining the herringbone-packing in the a−b plane. Such sliding dislocation effect leads to a variation in the molecular step heights, as shown in Figure 1b. The morphology of Pn thin films is also modulated by the underlying polycrystalline O_x−Au surfaces, resulting in height variations on the terrace surfaces.

Besides the surface morphology, we have also used STM to determine the energy level alignment of the underlying Pn/O_x−Au interfaces using the distance−voltage (z−V) spectroscopy.[13,14] As shown in Figure 2a, most areas show localized hole injection barriers lower than 0.3 eV, indicating nearly ohmic contact has been achieved at Pn/O_x−Au interfaces. After determining the work function of O_x−Au surfaces (4.7 eV, see Supporting Information) using ultraviolet spectroscopy (UPS), the energy diagram of Pn/O_x−Au interface is summarized in Figure 2b, which is compared with the diagram of Pn/air−Au interface with a Schottky-type contact of ~0.6 eV (Figure 2c).[3] Note that both Pn/O_x−Au and Pn/air−Au interfaces roughly follow the Schottky−Mott limit. The former is mainly

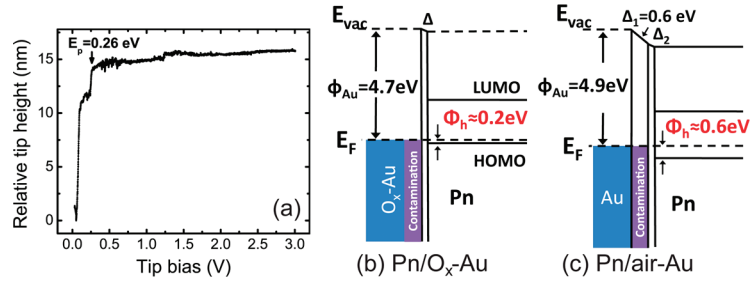

Figure 2. (a) A typical z−V spectrum of Pn thin film on O_x−Au substrate. Most areas of Pn/O_x−Au interfaces have hole injection barriers less than 0.3 eV. The spectrum was obtained with a constant current set point of 10 pA. (b and c) Energy level alignment at Pn/O_x−Au and Pn/air−Au interfaces, respectively. For Pn/O_x−Au, dipole formation is negligible due to the effective suppression of molecule−substrate interaction by surface oxidation. For Pn/air−Au, air exposure modifies the work function of Au from 4.9 to 4.3 eV by surface dipole formation (Δ_1). The subsequent evaporation of Pn produces very small dipole (Δ_2).

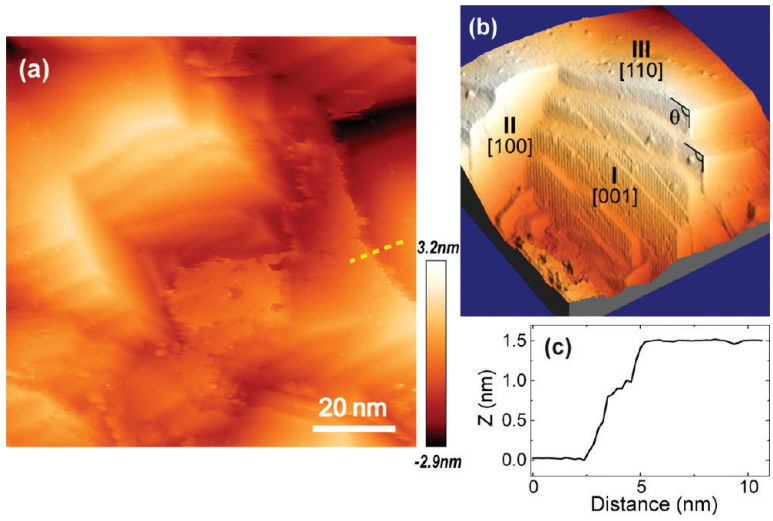

Figure 3. (a) STM image of Pn on 320 K O_x−Au. The lamellar structure corresponds to the single-crystal phase, while the faceted terraces on the right side have the thin-film phase structure with 1.5 nm molecular steps. (b) 3D STM image of the lamellar crystallites. Shading effect has been applied to visualize the details of three different crystal facets, namely, facets I, II, and III, respectively. (c) Line section of the "thin film phase" terrace. Scanning parameters: 100 × 100 nm²; V_{tip} = 2.8 V, I_t = 20pA.

due to the chemical modification of Au surface (the formation of Au−O bonds), while the latter is caused by air exposure.[15,16]

We further study the effect of substrate temperature on Pn thin film growth on O_x−Au. For these samples, the O_x−Au substrates are not cooled by RT N_2 during organic evaporation, resulting in a substrate temperature exceeding 45 °C during sample preparation. On SiO_2 surfaces, it is known that substrate temperatures above RT will lead to a mixed growth of both the thin-film phase and the single-crystal phase. Here, we observe a similar Pn growth mechanism on O_x−Au at elevated temperature.

In Figure 3, we show an area with dominant lamellar structure, a typical morphology of the single-crystal phase formed on the thin-film phase.[9] We also observe faceted terraces on the right part of the image with molecular steps of ~1.5 nm (Figure 3c), indicating that the single-crystal phase is nucleated on the thin-film phase. For the lamellar crystallites, three different crystal facets can be distinguished, as shown in Figure 3b by areas I, II, and III, respectively.

After zoom-in, facet I is identified as the [001] direction with a unit cell of a = 5.9 ± 0.2 Å, b = 7.7 ± 0.2 Å, and γ = 82 ± 3° using the STM topography image (Figure 4Ia) and the corresponding 2D fast Fourier transform (2D-FFT) image (Figure 4Ib). The acquired lattice parameters are consistent with the structure of Pn single crystal.[7] From the 2D-FFT image, the diffraction peaks corresponding to the herringbone stacking in the a−b plane, namely [$0^1/_20$] and [$^1/_200$], can also be distinguished. Note that the low resolution of the STM images is due to air exposure during sample transfer, but not related to the STM condition or scanning parameters. It is also noteworthy that the [001] plane of the lamellar crystallites is not perpendicular to the substrate surface, which is also observed on atomic flat SiO_2 surfaces. It cannot be attributed to the roughness of the underlying polycrystalline substrates.

Because of the herringbone packing structure in the a−b plane, Pn has a dentritic growth mode with two faster growth directions, that is [100] and [$\bar{1}$00], and four slow directions, that is, [110], [1$\bar{1}$0], [$\bar{1}$10], and [$\bar{1}\bar{1}$0].[17] Since the lamellar crystallites are elongated perpendicular to facet II, we can index this plane as [100]. Using the angle between facet II and III, $\theta \approx 135°$ as indicated in Figure 3b, we deduce the orientation of facet III to be [110].

The [100] orientation of facet II is confirmed by the STM topography and its 2D-FFT image, as shown in Figure 4 as IIa and IIb, respectively. From these two images, we determine an inter-row spacing of b = 7.9 ± 0.2 Å, consistent with the [100] surface direction. Surprisingly, we did not observe a similar row structure on facet III, which is expected for the [110] surface with a wider inter-row spacing than the [100] surface. Instead, a fine herringbone structure is recorded, as shown in Figure 4IIIa and Figure 4IIIb. Using the STM and 2D-FFT results, a unit cell of a = 5.8 ± 0.2 Å, b = 7.5 ± 0.1 Å, and γ = 91 ± 1° is deduced. This herringbone unit cell structure, especially the perpendicular unit cell angle, indicates that this is the [001] surface of the thin-film phase structure. Such an unexpected surface orientation of facet III implies that the thin-film phase can also nucleate and grow on the single-crystal phase, leading to

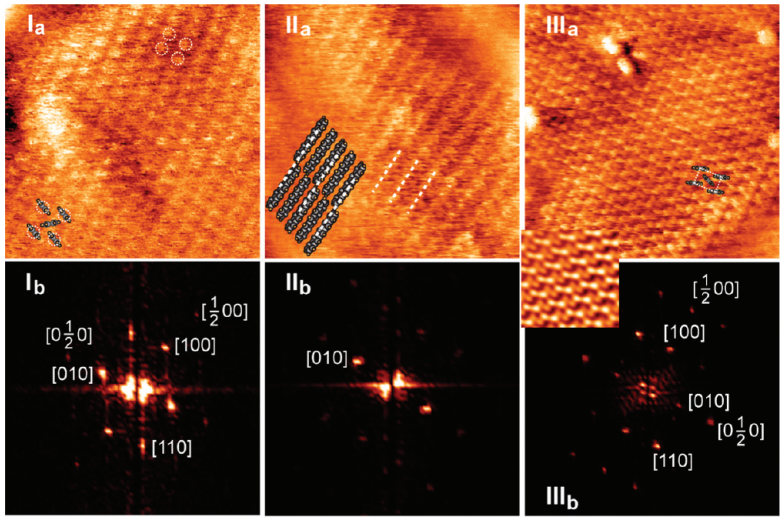

Figure 4. STM topography and the corresponding 2D-FFT images of facet I (I_a and I_b), facet II (II_a and II_b), and facet III (III_a and III_b). The inset in panel III_b shows the STM topography of facet III after 2D-FFT filtering. Scanning parameters: 10 × 10 nm²; V_{tip} = 2.8 V, I_t = 20pA.

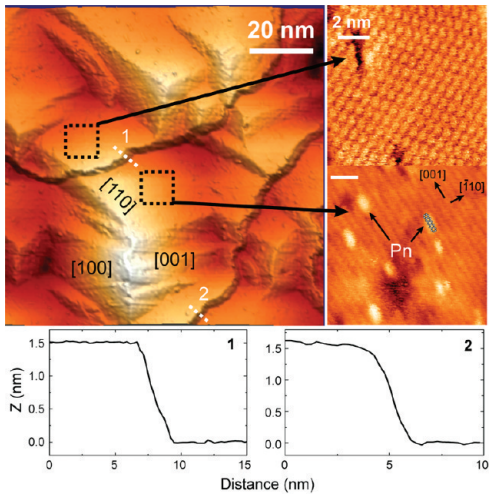

Figure 5. STM images of a different area with lamellar structure. The [110] surface shows a periodic row structure of 4.5 ± 0.2 Å. The lamellar crystallites are surrounded by thin-film phase terraces, characterized by ~1.5 nm molecular steps. After zoom-in, the [001] surface orientation of the facet terrace can be seen. Scanning parameters: V_{tip} = 2.3 V, I_t = 15pA.

a randomly mixed growth of the two crystalline phases. Note that this rodlike herringbone packing structure of the $a-b$ plane is quite different from the spherical shapes reported in the literature.[18] The above difference may be due to pick up of a Pn molecule by the STM tip during scanning, which will generally enhance the STM resolution.[19]

The intermixed growth of the single-crystal phase and the thin-film phase can also be seen in Figure 5. Using STM imaging on the [110] surface, the different crystalline surfaces of the lamellar crystallite have been marked accordingly. On the upper and right sides of this single crystal, thin-film phase terraces are found with molecular steps of ~1.5 nm, as shown in the inset 1 and 2 of Figure 5. STM on this terrace area gives a unit cell of a = 5.8 ± 0.2 Å, b = 7.5 ± 0.2 Å, and γ = 86 ± 2°. The nonrectangular lattice of the thin-film phase may be due to the polymorphism in Pn thin films or be caused by the tilted scanning surface. Note that there are planar adsorbed Pn molecules along the [001] direction on the [110] surface of the lamellar crystallite. The dimensions of these molecules are ~15.5 Å in length, ~9 Å in width, and ~1 Å in height.

Figure 6 shows another area dominated by the lamellar structure. STM scanning on the [110] surface, Figure 6I_a and Figure 6I_b, reveal a periodic row structure of 4.53 ± 0.2, in agreement with the unit cell of the single-crystal phase taking a = 5.9 ± 0.2 Å, b = 7.7 ± 0.2 Å, and γ = 82 ± 3° (Figure 4I). Note that there is a sudden switch-on of molecular resolution in Figure 6I_a, indicating the picking up of a Pn molecule by the STM tip. We next moved the STM tip to an area including both the [001] and [110] surface. The topography and 2D-FFT images on both surfaces agree very well with the corresponding crystalline orientations, as shown in Figure 6II_a, Figure 6II_b, and Figure 6II_c.

CONCLUSIONS

We prove STM is a unique and versatile tool for characterizing organic thin film growth. We show that O_2 plasma treatment of Au substrates can effectively decouple molecule−substrate interaction at Pn/O_x−Au interfaces. This effect allows Pn to grow on rough, polycrystalline O_x−Au surfaces in a quasi layer-by-layer fashion with well-defined thin-film phase structure and upright molecular orientation as a result of dominant intermolecule interaction. The surface plasma treatment also prevents the in-

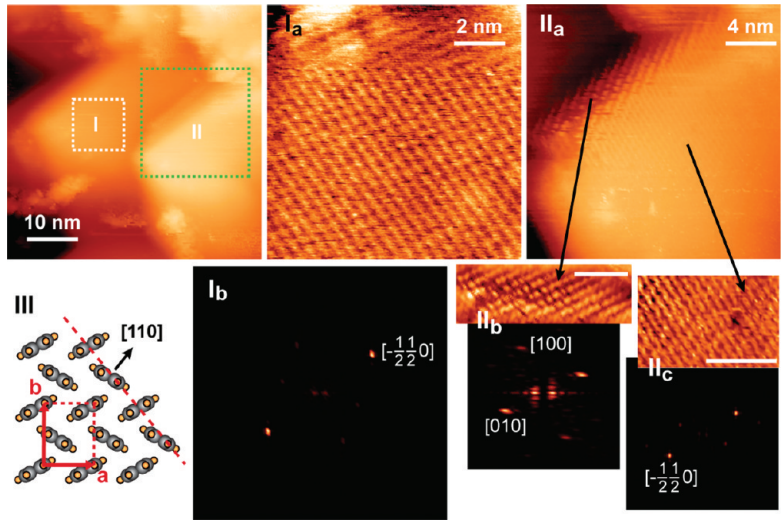

Figure 6. STM topography and the corresponding 2D-FFT images of another lamellar-structure area. STM results on [110], panels I_a and I_b, reveal a periodic row structure of 4.53 ± 0.2, agreeing well with the single-crystal unit cell parameters obtained in Figure 4I. In panels II_a, II_b, and II_c, molecular packing details on the [001] and [110] surfaces were shown, respectively. Panel III is a schematic diagram of the [110] surface, as seen from the [001] axis. Scanning parameters: V_{tip} = 2.3 V, I_t = 20pA.

terfacial dipole formation, leading to an ohmic contact at Pn/O_x−Au interfaces, as determined by STM distance−voltage spectroscopy. By elevating the substrate from RT to 320 K, we show an intermixed growth of the thin-film phase and the single-crystal phase, represented by terraced and lamellar structures,respectively, and determine the molecular packing parameters.

EXPERIMENTAL SECTION

The polycrystalline Au substrates were prepared by thermal evaporation of Au (99.99% purity) onto fresh cleaved mica with a background chamber pressure of 10^{-8} mbar and a deposition rate of 0.2−0.3 Å/s. The resulting 60 nm Au thin films show the typical granular surface morphology (see Supporting Information). Before transfer to a separate organic evaporation chamber (base pressure 10^{-7} mbar), the Au surfaces were treated by 50 W O_2 plasma for 120 s, which slightly oxidizes the Au substrates by introducing Au−O bonds at the surfaces.[20] Pn powder (99% sublimation purity) was obtained from Tokyo Chemical Industry Co. Pn thin films equivalent to 10−15 monolayers were thermally evaporated on the O_x−Au substrates with a deposition rate of 0.1 Å/s. Before the shutter was open, the source was annealed at around 120 °C for 1 h for outgassing lower vapor pressure contaminants and to achieve a more uniform temperature. The thin film samples were then loaded into a homemade high vacuum (10^{-8} mbar) STM system using a RHK scanning head for surface morphology and interfacial electronic structure characterizations.

Acknowledgment. We particularly acknowledge X. Y. Gao, D. C. Qi, and S. Chen for UPS and NEXAFS measurements. We thank C. Troadec for his help in our experiments.

Supporting Information Available: Polycrystalline Au surface; NEXAFS and UPS measurements of pentacene thin film on Ox−Au surface; surface morphology of pentacene thin films on Ox−Au and (C8-alkanethiol)−Au(111) substrates. This material is available free of charge *via* the Internet at http://pubs.acs.org.

REFERENCES AND NOTES

1. Witte, G.; Wöll, C. Growth of Aromatic Molecules on Solid Substrates for Applications in Organic Electronics. *J. Mater. Res.* **2004**, *19*, 1889.
2. Dimitrakopoulos, C. D.; Malenfant, P. R. L. Organic Thin Film Transistors for Large Area Electronics. *Adv. Mater.* **2002**, *14*, 99.
3. Zheng, Y.; Qi, D. C.; Chandrasekhar, N.; Gao, X. Y.; Troadec, C.; Wee, A. T. S. Effect of Molecule−Substrate Interaction on Thin-Film Structures and Molecular Orientation of Pentacene on Silver and Gold. *Langmuir* **2007**, *23*, 8336.
4. Söhnchen, S.; Lukas, S.; Witte, G. Epitaxial Growth of Pentacene Films on Cu(110). *J. Chem. Phys.* **2004**, *121*, 525.
5. Drummy, L. F.; Martin, D. C. Thickness-Driven Orthorhombic to Triclinic Phase Transformation in Pentacene Thin Films. *Adv. Mater.* **2004**, *7*, 903.
6. Stöhr, M.; Gabriel, M.; Möller, R. Analysis of the Three-Dimensional Structure of a Small Crystallite by Scanning Tunneling Microscopy: Multilayer Films of 3,4,9,10-Perylenetetracarboxylic-Dianhydride (PTCDA) on Cu(110). *Europhys. Lett.* **2002**, *59*, 423.
7. Campbell, R. B.; Robertson, J. M.; Trotter, J. Crystal and Molecular Structure of Pentacene. *Acta Crystallogr.* **1961**, *14*, 705.
8. Ruiz, R.; Mayer, A. C.; Malliaras, G. G.; Nickel, B.; Scoles, G.; Kazimirov, A.; Kim, H.; Headrick, R. L.; Islam, Z. Structure of Pentacene Thin Films. *Appl. Phys. Lett.* **2004**, *85*, 4926.
9. Bouchoms, I. P. M.; Schoonveld, W. A.; Vrijmoeth, J.; Klapwijk, T. M. Morphology Identification of the Thin Film Phases of Vacuum Evaporated Pentacene on SiO_2 Substrates. *Synth. Met.* **1999**, *104*, 175.
10. Käfer, D.; Ruppel, L.; Witte, G. Growth of Pentacene on Clean and Modified Gold Surfaces. *Phy. Rev. B* **2007**, *75*, 085309.
11. Heringdorf, F. M. Z.; Reuter, M. C.; Tromp, R. M. Growth Dynamics of Pentacene Thin Films. *Nature* **2001**, *412*, 517.
12. Kang, J. H.; Zhu, X. Y. Pi-Stacked Pentacene Thin Films Grown on Au(111). *Appl. Phys. Lett.* **2003**, *82*, 3248.
13. Alvarado, S. F.; Seidler, P. F.; Lidzey, D. G.; Bradley, D. D. C. Direct Determination of the Exciton Binding Energy of Conjugated Polymers Using a Scanning Tunneling Microscope. *Phy. Rev. Lett.* **1998**, *81*, 1082.
14. Alvarado, S. F.; Rossi, L.; Müller, P.; Seidler, P. F.; Reiss, W. STM-Excited Electroluminescence and Spectroscopy on Organic Materials for Display Applications. *IBM J. Res. Dev.* **2001**, *45*, 89.
15. Greczynski, G.; Fahlman, M.; Salaneck, W. R. Electronic Structure of Hybrid Interfaces of Poly(9,9-dioctylfluorene). *Chem. Phys. Lett.* **2000**, *321*, 379.
16. Grobosch, M.; Knupfer, M. Charge-Injection Barriers at Realistic Metal/Organic Interfaces: Metals Become Faceless. *Adv. Mater.* **2007**, *19*, 754.
17. Voigt, M.; Dorsfeld, S.; Volz, A.; Sokolowski, M. Nucleation and Growth of Molecular Organic Crystals in a Liquid Film under Vapor Deposition. *Phy. Rev. Lett.* **2003**, *91*, 026103.
18. Thayer, G. E.; Sadowski, J. T.; zu Heringdorf, F. M.; Sakurai, T.; Tromp, R. M. Role of Surface Electronic Structure in Thin Film Molecular Ordering. *Phy. Rev. Lett.* **2005**, *95*, 256106.
19. Repp, J.; Meyer, G.; Stojković, S. M.; Gourdon, A.; Joachim, C. Molecules on Insulating Films: Scanning-Tunneling Microscopy Imaging of Individual Molecular Orbitals. *Phy. Rev. Lett.* **2005**, *94*, 026803.
20. Kim, W. K.; Lee, J. L. Effect of Oxygen Plasma Treatment on Reduction of Contact Resistivity at Pentacene/Au Interface. *Appl. Phys. Lett.* **2006**, *88*, 262102.